

Gain control by layer six in cortical circuits of vision

Shawn R. Olsen^{1*}, Dante S. Bortone^{1*}, Hillel Adesnik¹ & Massimo Scanziani¹

After entering the cerebral cortex, sensory information spreads through six different horizontal neuronal layers that are interconnected by vertical axonal projections. It is believed that through these projections layers can influence each other's response to sensory stimuli, but the specific role that each layer has in cortical processing is still poorly understood. Here we show that layer six in the primary visual cortex of the mouse has a crucial role in controlling the gain of visually evoked activity in neurons of the upper layers without changing their tuning to orientation. This gain modulation results from the coordinated action of layer six intracortical projections to superficial layers and deep projections to the thalamus, with a substantial role of the intracortical circuit. This study establishes layer six as a major mediator of cortical gain modulation and suggests that it could be a node through which convergent inputs from several brain areas can regulate the earliest steps of cortical visual processing.

Primary sensory areas in the cerebral cortex are composed of a stack of six neuronal layers¹. Anatomical and physiological data indicate that these layers are interconnected through vertical excitatory axons^{2–6}, suggesting that sensory processing in any given layer may be modulated by activity in several other layers. However, so far the exact contribution of each layer to cortical processing is unclear.

Here we address the role of layer six (L6) in mouse visual cortex, whose excitatory neurons not only project to more superficial layers but also to the primary sensory thalamic nuclei^{3,7–11}, the main source of sensory input to the cortex (Fig. 1a). L6 may thus influence cortical sensory responses directly through intracortical projections and indirectly through corticothalamic projections. Corticothalamic projections were reported to be both suppressive and facilitatory on thalamic activity, depending on the precise alignment between L6 and thalamic neurons (for reviews see refs 12–16). By contrast, how sensory responses in cortex are affected by L6 activity has remained largely unexplored^{17,18}. Furthermore, the relative contribution of intracortical versus corticothalamic projections in modulating cortical responses is currently unknown. The paucity of information is due to the lack of experimental tools for selectively manipulating activity in L6 without directly perturbing other cortical layers.

L6 neurons of the *Ntrsl*-Cre GN220 line

To control the activity of L6 we took advantage of a Cre-recombinase Bac transgenic mouse line that is reported to selectively label L6 neurons (NTSR1-Cre GN220)¹⁹. In the forebrain of these mice Cre expression was restricted to excitatory L6 neurons of the cerebral cortex (Fig. 1b and Supplementary Fig. 1). In primary visual cortex (V1) these neurons represented ~65% of the L6 excitatory neuronal population and, consistent with classification of L6 neurons in this region¹, could be subdivided into two morphologically distinct categories: those whose apical dendrites ended in L4 and those that extended to L1 (Fig. 1b and Supplementary Fig. 1g, h). Furthermore, consistent with the corticothalamic projections originating from L6 in V1 (ref. 8), Cre-expressing neurons projected to the dorsolateral geniculate nucleus (dLGN; the primary thalamic visual nucleus) and the nucleus reticularis thalami (NRT; the main thalamic inhibitory nucleus) (Fig. 1b and

Supplementary Fig. 1d, e). Thirty-five percent of L6 excitatory neurons in V1 did not express Cre and these were morphologically distinct from the Cre-expressing population (Supplementary Fig. 1g).

To manipulate the activity of L6 neurons we conditionally expressed the light-sensitive cation channel channelrhodopsin 2 (ChR2)^{20,21} in V1 using viral injection into NTSR1-Cre mice (Supplementary Fig. 2a). A linear multichannel probe recorded the spiking activity of neurons located across the vertical depth of cortex. Light-emitting diode (LED) illumination of the cortical surface for 500 ms with blue light (470 nm) increased the activity of L6 neurons in V1 of anaesthetized animals (Fig. 1c–e and Supplementary Fig. 2b). This increase was not due to direct stimulation of the retina by the LED as it was absent in uninjected animals (Supplementary Fig. 2g).

L6 activity suppresses other layers

To determine how L6 activation affects visual responses in other layers, we presented drifting gratings, and alternated control trials (visual stimulus only) with trials in which L6 was photostimulated (Fig. 1c). Notably, photostimulation of L6 rapidly and reversibly suppressed visually evoked multi-unit activity throughout the depth of the cortex (Fig. 1d). L6 photostimulation also reduced spontaneous activity (Supplementary Fig. 3d, e). This effect was absent in uninjected animals (Supplementary Fig. 2g). The suppressive action of L6 was similar across L2/3, L4 and L5 and was monotonic (Fig. 1e,f): that is, increasing L6 activity by increasing illumination intensity progressively suppressed visual responses, eventually abolishing nearly all evoked activity (strongest illumination reduced activity by $81 \pm 5\%$, $84 \pm 3\%$, and $84 \pm 3\%$ for L2/3, L4 and L5, respectively; $P < 10^{-5}$). Because multi-unit activity is dominated by neurons with high firing frequencies, we determined the effect of L6 photostimulation on isolated single units whose average visually evoked firing rate varied over a 20-fold range. Isolated units were suppressed by L6 photostimulation (Fig. 1g), irrespective of their firing rates (Fig. 1h; 91.1% of units were suppressed and 7.8% were facilitated, and all facilitated units were fast-spiking, putative inhibitory cells (Supplementary Fig. 4a–d). Furthermore, in the same way as for multi-unit activity, L6 photostimulation monotonically suppressed single units (Fig. 1i, j; strongest

¹Howard Hughes Medical Institute, Center for Neural Circuits and Behavior, Neurobiology Section and Department of Neuroscience, University of California San Diego, La Jolla, California 92093-0634, USA.

*These authors contributed equally to this work.

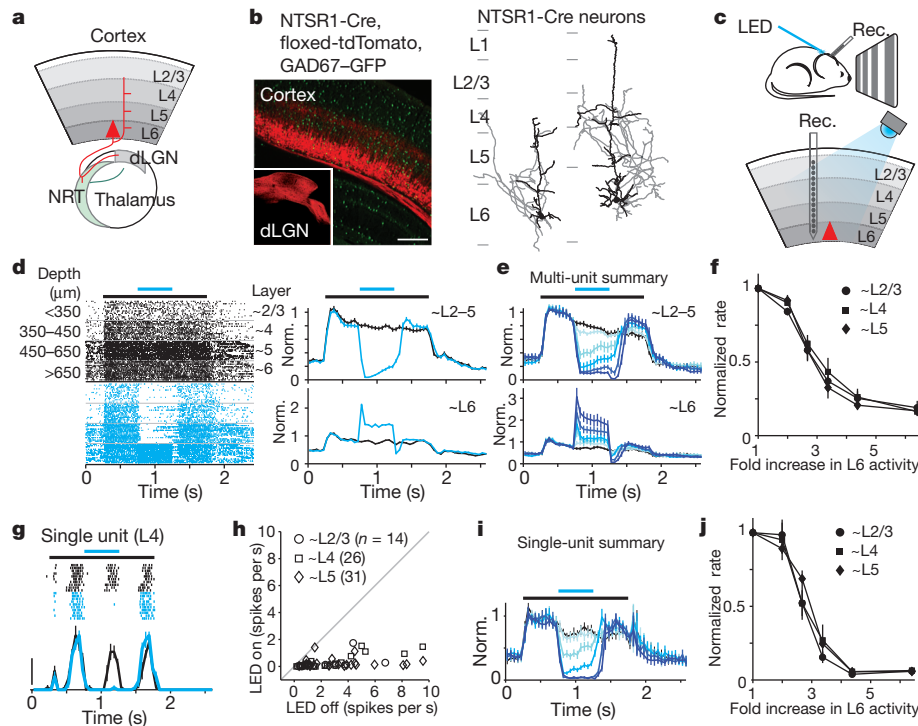


Figure 1 | Photostimulation of L6 suppresses visual responses in the other layers. **a**, Schematic of L6 projections. Red triangle represents an L6 pyramidal neuron. **b**, Left, coronal section of V1 from an NTSR1-Cre, floxed-tdTomato, GAD67-GFP mouse. Inset, L6 projection to dLGN (V1 of NTSR1-Cre mouse was injected with floxed-tdTomato virus). Scale bar, 250 μm (125 μm for inset). Right, the two types of L6 neurons that are labelled by the NTSR1-Cre line. Black, dendrites; grey, axons. **c**, Schematic of experimental setup. Rec., recording probe. **d**, Cortical visual responses with (blue) and without (black) L6 photostimulation. Left, raster plot of multi-unit activity grouped by depth. Control and photostimulation trials were interleaved but are separated here for

illumination reduced activity by $91 \pm 4\%$, $93 \pm 2\%$, and $92 \pm 2\%$ for L2/3, L4 and L5, respectively; $P < 10^{-9}$). Thus, these data show that stimulation of L6 excitatory neurons suppresses visually evoked responses in L2/3, L4 and L5 of V1.

L6 activity does not affect tuning

Like in other mammals, neurons in mouse V1 differentially respond to gratings of different orientations^{22,23}. We determined whether L6 stimulation affects the orientation tuning of V1 neurons. We generated tuning curves by presenting gratings drifting in 8–12 different directions and alternated control trials with trials in which L6 was photostimulated (Fig. 2a, b). We used a low LED intensity to suppress cortical visual responses partially, and considered units that were suppressed by between 10% and 75% (average suppression $42 \pm 3\%$, $n = 55$). Tuning curves of individual, isolated units were averaged into a population tuning curve (Fig. 2b, d; see methods). Remarkably, photostimulation of L6 resulted in the precise scaling of the tuning curve; that is, it reduced visually evoked responses by a similar fraction irrespective of presented orientation. This is clearly illustrated by plotting the normalized firing rates of the population tuning curve under control versus L6 photostimulation conditions (Fig. 2e). The data points fit well with a line whose slope is 0.56 and intercepts the y axis close to the origin. Thus, photostimulation of L6 did not affect preferred orientation, tuning width or the orientation selectivity index (OSI) of cortical neurons throughout L2/3, L4 and L5 (Fig. 2c; for L2/3, L4 and L5, respectively, the mean change in preferred orientation was $3 \pm 3^\circ$ ($P = 0.22$), $0 \pm 5^\circ$ ($P = 0.9$) and $-4 \pm 5^\circ$ ($P = 0.48$), mean change in tuning width was $-1 \pm 4^\circ$ ($P = 0.8$), $6 \pm 4^\circ$ ($P = 0.15$) and $-6 \pm 6^\circ$ ($P = 0.3$), and mean change in OSI was -0.09 ± 0.07 ($P = 0.23$),

clarity. Black bar, visual stimulus (1.5 s); blue bar, LED illumination (0.5 s). Right, normalized (Norm.) peristimulus time histogram (PSTH); top, upper layers; bottom, L6. **e**, Summary ($n = 6$ experiments). The control is shown in black and increasing LED intensities in darker blues. **f**, Suppression of multi-unit activity with increasing L6 activity. **g**, Visual response of a single L4 unit with (blue) and without (black) L6 photostimulation. Scale bar, 20 spikes per s. **h**, Response of each regular spiking unit with and without strong photostimulation of L6. **i**, Average normalized PSTH ($n = 47$ units tested with 5 LED intensities). Colours are the same as in **e**. **j**, Suppression of single-unit activity. Error bars, mean \pm s.e.m.

0.7 ± 0.04 ($P = 0.14$), -0.06 ± 0.05 ($P = 0.22$)). L6 photostimulation also resulted in a scaling of V1 responses to stimuli of increasing contrast (the contrast response function; Supplementary Fig. 5b). These data demonstrate that in primary visual cortex L6 selectively controls the gain of cortical responses to visual stimuli.

A potential concern in stimulating L6 with ChR2 is that the spatially uniform activation and the temporal pattern generated in L6 neurons may differ from visually evoked activity patterns, and thus the physiological activity of L6 neurons and L6 photostimulation may affect cortical activity in different ways. Furthermore, anaesthesia may change the impact of L6 on cortical responses to sensory stimuli. To address these issues, we optogenetically suppressed visually evoked activity in L6 in awake animals and determined the resulting effect on more superficial layers (Supplementary Fig. 6). Animals were head fixed but otherwise kept unrestrained on a passive circular treadmill (see Methods). L6 activity was suppressed using conditionally expressed light-sensitive hyperpolarizing opsins archaeorhodopsin²⁴ and halorhodopsin 3.0 (NpHR3.0) (ref. 25). LED illumination with amber light (590 nm), although reducing visually evoked L6 activity by $\sim 30\%$ (Supplementary Fig. 6e), significantly facilitated visual responses of isolated units throughout the other layers (Fig. 2f, g and Supplementary Fig. 6). The facilitation was not due to direct LED illumination of the retina, as it was absent in uninjected animals (Supplementary Fig. 6f). Thus, suppression of L6 facilitates visually evoked activity in L2/3, L4 and L5, indicating that even physiologically generated L6 activity exerts a suppressive action onto these layers. Furthermore, suppression of L6 resulted in the precise scaling of the tuning curve (for the tuning curve analysis we considered units that were facilitated by at least 10% (average facilitation $41 \pm 7\%$, $n = 52$)).

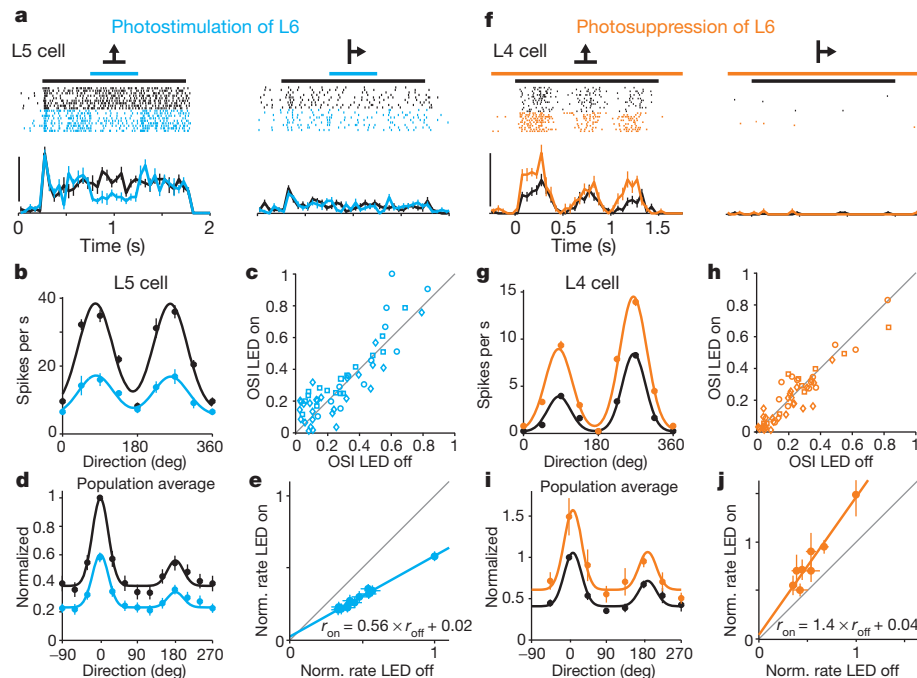


Figure 2 | L6 bidirectionally modulates the gain of visual responses without altering tuning. **a**, Visual responses of an L5 neuron with (blue) and without (black) L6 photostimulation. Raster plots and peristimulus time histograms for two out of eight tested visual stimulus directions. Scale bar, 40 spikes per s. **b**, Tuning curves for the neuron in (a). **c**, The OSI for each neuron with and without photostimulation of L6. **d**, Population tuning curve with (blue) and without (black) L6 photostimulation ($n = 55$). Black curve, fit using the sum of two Gaussians; blue curve, black curve scaled by the slope of linear fit in **e**. **e**, Control response plotted against response with L6 photostimulation (data from **c**). Blue, linear fit ($r^2 = 0.98$). Black bar, visual stimulus (1.5 s); blue bar,

LED illumination (0.5 s). **f**, Visual response of an L4 neuron with (orange) and without (black) L6 photosuppression. Scale bar, 50 spikes per s. Orange bars, illumination with an amber-coloured LED (1.95 s); black bar, visual stimulation (1.5 s). **g**, Tuning curves for neuron in (f). **h**, OSI for each isolated unit with and without photosuppression of L6. **i**, Population tuning curves with and without L6 photosuppression ($n = 52$). Black curve, fit using sum of two Gaussians; orange curve, black curve scaled by slope of linear fit in **j**. **j**, Control response plotted against response with L6 photostimulation (data from **i**). Orange, linear fit ($r^2 = 0.92$). Error bars, mean \pm s.e.m.

The plot of normalized firing rates under control versus L6 photosuppression conditions was well fit by a line whose slope is 1.4 and intercepts the y axis very close to the origin (Fig. 2j). Consistent with this, suppressing L6 did not affect preferred orientation, tuning width or orientation selectivity (Fig. 2h; for L2/3, L4 and L5, respectively, the mean change in preferred orientation was $2 \pm 3^\circ$ ($P = 0.41$), $0 \pm 2^\circ$ ($P = 0.95$) and $-4 \pm 4^\circ$ ($P = 0.35$) degrees, mean change in tuning width was $-2 \pm 4^\circ$ ($P = 0.68$), $0 \pm 3^\circ$ ($P = 0.94$) and $-1 \pm 4^\circ$ ($P = 0.77$) degrees, and mean change in OSI was -0.01 ± 0.03 ($P = 0.22$), 0.02 ± 0.02 ($P = 0.50$) and -0.03 ± 0.03 ($P = 0.22$)). Taken together, these results demonstrate that visually driven L6 activity in awake animals controls the gain of cortical responses to visual stimuli.

L6 intracortical and subcortical pathways

Two pathways could potentially mediate the suppression exerted by L6 on cortical activity. On one hand, L6 neurons project to the thalamus, where they can influence visually generated activity before it even reaches the cortex. On the other hand, L6 neurons also project to more superficial layers where they could directly modulate cortical activity. We addressed the impact of both projections. We performed extracellular recordings from the dLGN while photostimulating L6 in V1 (Fig. 3a). dLGN relay neurons were identified based on their visual response properties and characteristic firing pattern (Supplementary Fig. 7d). Photostimulation of L6 led to a rapid, reversible and monotonic reduction of visually evoked activity in dLGN relay neurons (Fig. 3b, c; strongest illumination: $76 \pm 4\%$ reduction; $P < 10^{-10}$, $n = 32$), without, however, markedly modifying their firing mode (burst prevalence: $12 \pm 6\%$ in control; $6 \pm 3\%$ after reducing dLGN activity by 30% with L6 photostimulation, $P = 0.08$; Supplementary Fig. 7e, f). This indicates that L6 stimulation suppresses

dLGN activity. To test whether visually evoked activity in L6 also suppresses dLGN activity we silenced the cortex optogenetically (by photostimulating parvalbumin-expressing inhibitory neurons in V1 with Chr2; see Methods and Supplementary Fig. 8). Consistent with the suppressive action of L6 stimulation on dLGN, silencing the cortex strongly facilitated dLGN activity (Fig. 3d–f; average facilitation $87 \pm 25\%$ ($P = 0.002$, $n = 18$)). *In vitro* recordings demonstrated that the suppressive action of L6 was due to the generation of disynaptic inhibition onto dLGN relay neurons, at least in part through the recruitment of NRT inhibitory neurons (and possibly through the recruitment of local inhibitory neurons in dLGN²⁶) (Supplementary Fig. 9). Thus, these results reveal that L6 can effectively suppress visual responses in the dLGN.

If L6 suppresses cortical visual responses indirectly, by suppressing the dLGN, this suppression should precede V1 suppression by a few milliseconds. We tested this prediction by performing simultaneous recordings from both dLGN and V1 and compared the onset of suppression in these two structures upon L6 photostimulation (Fig. 3g). Surprisingly, cortical suppression preceded dLGN suppression by a few milliseconds (Fig. 3h). This result suggests that L6 activity may suppress cortical visual responses through an alternative circuit. Because L6 neurons send axons to the upper layers of cortex we tested whether these projections can suppress cortical activity independently of the corticothalamic projections. For this, we performed *in vitro* whole-cell recordings from neurons in L2/3, L4, L5 and L6 in coronal slices of V1 (Fig. 4a); this slicing plane disconnects V1 from dLGN.

Photostimulation of L6 *in vitro* generated both excitatory and inhibitory postsynaptic currents (EPSCs and IPSCs, respectively) onto L2/3, L4, L5 and L6 pyramidal cells (L6 recordings included only those pyramidal cells not expressing Chr2) (Fig. 4b). IPSCs were of disynaptic (or polysynaptic) origin as they were entirely blocked by

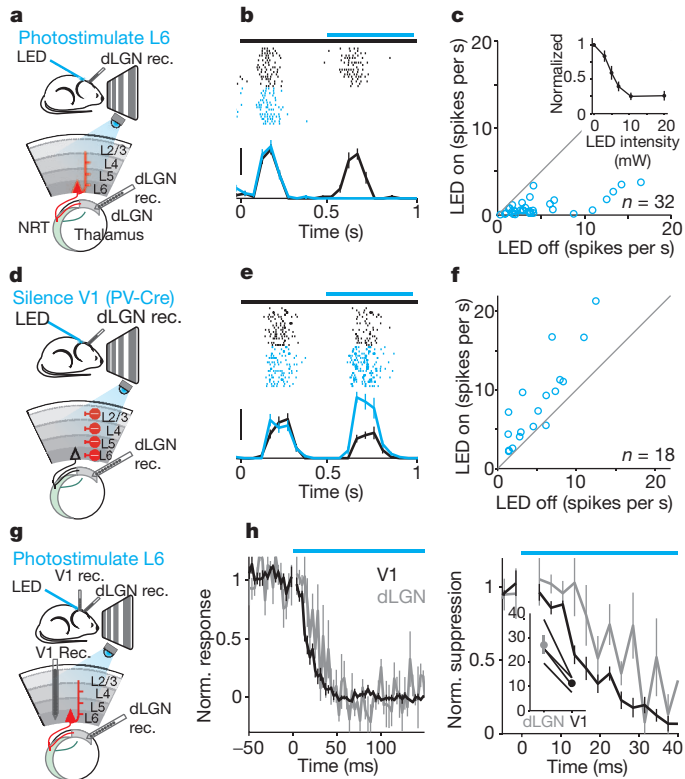


Figure 3 | Photostimulation of L6 suppresses cortex faster than it suppresses dLGN. **a**, Schematic of the experimental setup. **b**, Visual response of dLGN unit with (blue) and without (black) L6 photostimulation. Scale bar, 20 spikes per s. Black bar, visual stimulus (1 s); blue bar, LED illumination (0.5 s). **c**, Average response of each dLGN unit with and without L6 photostimulation. Inset, monotonic suppression of dLGN. **d**, Schematic of setup for silencing V1 by photostimulation of parvalbumin inhibitory neurons. **e**, Visual response of dLGN unit with and without photo-silencing of V1. Scale bar, 30 spikes per s. Black bar, visual stimulus (1 s); blue bar, LED illumination (0.5 s). **f**, Average response of each dLGN unit with and without cortical silencing. **g**, Schematic of experimental setup. **h**, Left, time-course of L6-mediated suppression of dLGN (grey) and V1 (black) ($n = 4$). Residual response during maximal suppression set to zero (see Methods). Bin size, 3 ms. Right, the same data on an expanded timescale. The first bin at LED onset was blanked to remove LED-induced artefact. Inset, time to suppression exceeding two standard deviations from baseline activity in dLGN and V1 for four experiments ($P = 0.012$). Error bars, mean \pm s.e.m. Inset, y-axis units are ms.

glutamatergic antagonists (Supplementary Fig. 10b). Furthermore, the activity pattern generated by L6 photostimulation was similar to the activity pattern generated *in vivo* (Supplementary Fig. 2b, h). IPSCs were larger than EPSCs, despite the fact that both currents were recorded with a similar driving force (IPSCs were recorded near the reversal potential for EPSCs and vice versa). Indeed, excitatory charge accounted for only 10% or less of the total charge, depending on the layer (Fig. 4c) or sublayer (Supplementary Fig. 10c, d). These results show that V1 contains the necessary circuitry for L6 to generate disinaptic inhibition onto L2/3, L4, L5 and onto itself.

To determine whether L6 can suppress neuronal spiking across L2/3, L4, L5 and L6 through these disinaptic IPSCs, we performed current-clamp recordings in the perforated patch configuration (to preserve the intracellular ionic composition) and triggered spiking by injecting depolarizing current pulses. Photostimulation of L6 significantly suppressed firing of pyramidal cells across all layers (Fig. 4d; firing rate was reduced by $48 \pm 10\%$, $84 \pm 7\%$, $55 \pm 19\%$ and $75 \pm 11\%$ for L2/3, L4, L5 and L6, respectively; $P \leq 0.01$). To rule out the possibility that this suppression was a result of uniformly activating large portions of L6 we restricted the area of activation to a small spot of approximately $100 \mu\text{m}$ in diameter while recording

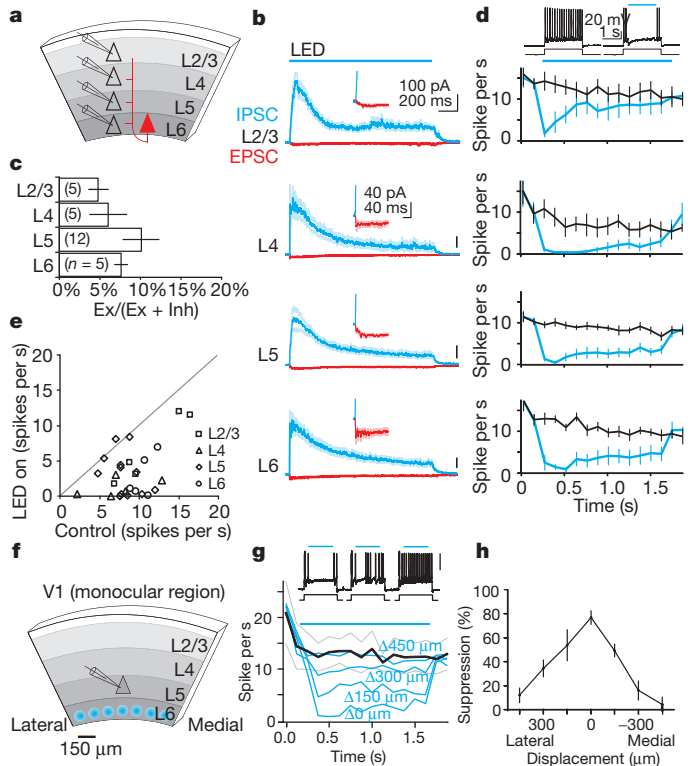


Figure 4 | Photostimulation of L6 recruits intracortical synaptic inhibition. **a**, Schematic of *in vitro* experimental setup. **b**, Average IPSCs (blue) and EPSCs (red) recorded in pyramidal cells during photostimulation of L6. Synaptic currents are averages of $n = 5$ –12 cells. Inset, onset of EPSC. **c**, Histogram of excitatory charge as a percentage of total charge. Ex, excitation; Inh, inhibition. **d**, Traces show perforated patch recording from L5 pyramidal cell in response to depolarizing current injection with (right) and without (left) L6 photostimulation. Graphs, spike rate with and without L6 photostimulation. **e**, Average spike rate in control versus spike rate with L6 photostimulation for each cell. **f**, Schematic of experimental setup for focal photostimulation. **g**, Traces, spiking of L5 pyramidal cell to depolarizing current injection with focal photostimulation of L6 at three progressively more distant positions (left to right). Graph shows spike rate in control (black) and with focal photostimulation of L6 (blue) ($n = 4$). Delta indicates the medial or lateral distance from the radial axis through the recording site. **h**, Percentage of spike suppression plotted against horizontal displacement. Error bars, mean \pm s.e.m.

from a L5 neuron (Fig. 4f). Even when activating a restricted area of L6, the firing of L5 neurons was robustly suppressed (Fig. 4g). The suppression was maximal when L6 photostimulation was aligned with the recorded L5 neuron along the cortical radial axis, and decreased progressively as the photostimulation spot was translated tangentially (Fig. 4g, h). These results demonstrate that V1 can efficiently suppress activity in L2/3, L4, L5 and L6 in the absence of thalamus.

Major role of L6 intracortical circuits

Taken together, these results indicate that L6 can modulate cortical responses to visual stimuli through two independent circuits: indirectly, through the corticothalamic circuit and directly, through the intracortical circuit. To test whether one of these two circuits has a dominant role, we examined how much of the V1 suppression is predicted by dLGN suppression. We first established the transfer function between dLGN and V1. For this we performed simultaneous *in vivo* recordings from these two structures while presenting full-field drifting gratings of varying contrasts to obtain contrast response functions for the dLGN and V1 (Fig. 5a, b). By plotting dLGN versus V1 activity at each contrast we obtained the transfer function from dLGN to V1, which provides the response of V1 to various levels of dLGN activity (Fig. 5c). Finally, we presented the strongest contrast and photostimulated L6 to reduce dLGN activity while simultaneously monitoring V1 activity.

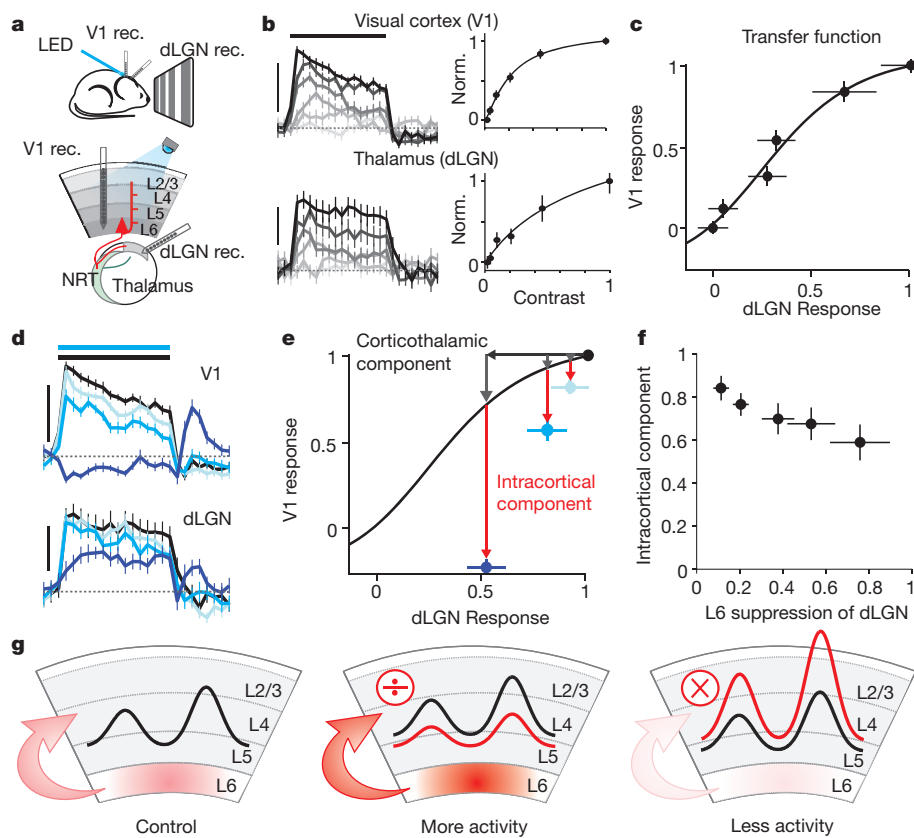


Figure 5 | L6 suppresses upper layers largely through intracortical circuits. **a**, Schematic of experimental setup. **b**, Simultaneously recorded multi-unit responses to increasing contrasts (light to dark) in V1 (top) and dLGN (bottom). All spikes that were recorded above L6 ($\leq 650 \mu\text{m}$) were included in V1 multi-unit activity. Scale bar, 200 spikes per s for V1; 100 spikes per s for dLGN. Black bar, visual stimulus (1.5 s). Dotted line, baseline activity. Right, contrast–response functions. **c**, dLGN–V1 transfer function derived by plotting normalized response in V1 versus dLGN (from **b**). Fit, hyperbolic ratio function. **d**, Simultaneously recorded multi-unit responses to maximal contrasts in V1 and dLGN without photostimulation (black) or while photostimulating L6 with increasing LED intensities (progressively darker blue). Same experiment as in **b** and **c**. Black bar, visual stimulus (1.5 s); blue bar, LED illumination (1.5 s). Scale bars are the same as in **b**. **e**, V1 versus dLGN response to maximal contrast under control condition (black data point) or during three progressively stronger photostimulations of L6 (light, medium and dark blue, data from **d**). V1 responses are suppressed more than predicted by transfer function (red arrows) even for photostimulations that reduce dLGN activity only $\sim 10\%$ (light blue). **f**, Average intracortical component of suppression as a function dLGN suppression ($n = 5$ experiments). Intracortical component (red arrow in **e**) is quantified as a fraction of total V1 suppression (grey arrows plus red arrows in **e**). **g**, Schematic of the main finding. Error bars, mean \pm s.e.m.

We reasoned that if the ensuing reduction of V1 activity matches the reduction predicted by the transfer function, the modulation of cortical responses by L6 is mainly due to dLGN suppression by the corticothalamic circuit. However, if the reduction in V1 activity exceeds that predicted by the transfer function, the additional reduction can be attributed to the intracortical circuit. We reduced dLGN activity by $\sim 10\%$, 20% and 50% through activation of L6 with three progressively stronger illuminations (Fig. 5d). Notably, even the smallest reduction in dLGN activity (10%) was accompanied by a reduction in V1 activity that largely exceeded that predicted by the transfer function (Fig. 5e). Furthermore, a 50% suppression of dLGN activity was accompanied by a complete suppression of visually evoked activity in V1. In this experiment a large fraction of V1 suppression (73% averaged over five LED levels) exceeded the transfer function prediction and must therefore be attributed to the intracortical circuit (average intracortical component over all experiments $73 \pm 5\%$, $n = 5$; Fig. 5f). Furthermore, given the relatively minor effects on the prevalence of burst firing in dLGN neurons (Supplementary Fig. 7f), this effect cannot be attributed to a change in the firing pattern of dLGN neurons. These results indicate that L6 suppresses cortical responses to visual stimuli mainly through intracortical circuits.

Discussion

Taken together, this study shows that L6 modulates visually evoked activity across L2/3, L4 and L5. This modulation occurs continuously through visually driven L6 activity, as shown in awake animals, and does not affect orientation tuning indicating that L6 selectively controls the gain of cortical visual responses. Finally, despite suppression of the dLGN, cortical gain control by L6 is executed largely by intracortical circuits.

Response gain modulation is a fundamental cortical operation²⁷ that is crucially involved in sensory representation and sensorimotor integration. For example, visual responses in parietal cortex are gain modulated by gaze direction²⁸. Furthermore, gain modulation may underlie

the effects of attention on cortical responses to visual stimuli^{29,30}. However, the neuronal circuits that implement this operation have remained largely unknown. Identifying L6 as a contributor to cortical response gain modulation is an important step in dissecting the specific functions of distinct circuits in cortical processing. The suppressive action of L6 that is described here markedly differs from the facilitatory impact of other layers on cortical activity^{3,31,32} (for example, L2/3 facilitates L5 (ref.³²)) and points towards a very distinct function of different layers in sensory processing. The cortical GABAergic interneuron subtype (or subtypes)^{33,34} that is recruited by L6 activity and mediates the reported suppressive effect remains to be identified, but may include fast spiking neurons (Supplementary Fig. 4). Although the exact synaptic mechanisms underlying gain control by L6 remains to be elucidated, either a proportional change in excitation and inhibition^{35,36} or the modulation of only one of the two opposing conductances³⁷ may underlie the operation. The columnar organization of L6 pyramidal cell projections to more superficial layers¹⁰ ensures that L6-mediated suppression is restricted to the cortical domains that are directly above the activated L6 region (Fig. 4g, h). This topographic organization could allow the cortex to differentially modulate the gain of V1 responses to stimuli located in distinct regions of visual space.

L6 has been suggested to contribute to ‘end inhibition’, the suppression of cortical responses by bars above a given size¹⁷. The powerful inhibitory currents generated by L6 onto more superficial pyramidal cells may represent the underlying cellular mechanism.

Previous studies addressing the role of corticothalamic feedback projections through focal pharmacological perturbation of L6 neurons have typically reported a facilitation of functionally or topographically aligned thalamic neurons overlaid by broader surround suppression¹⁶, resulting in changes to both spatial and temporal tuning properties of these neurons^{15,38–41}. Our data obtained using full-field visual stimulation are consistent with this model, in which spatial summation of individual inhibitory surrounds will result in a net suppressive effect of the corticothalamic feedback projection. Future studies combining

optogenetic approaches with focal stimulation of visual space will reveal how fine-scale corticothalamic circuits^{39,42} interact with intracortical L6 circuits to influence visual processing in the cortex.

L6 in V1 receives convergent inputs from a variety of brain regions, including higher cortical areas⁴³ as well as thalamus¹¹. These various brain regions could thus influence, through L6, the gain of visual responses during the very initial steps of visual cortical processing.

METHODS SUMMARY

ChR2, archaerhodopsin and NpHR3.0 were conditionally expressed in mouse V1 via stereotactic injection of adenoassociated viruses into NTSR1-Cre mice¹⁹. For recordings under anaesthesia, mice were injected with 5 mg kg⁻¹ chlorprothixene and 1.2 g kg⁻¹ urethane. For awake experiments, a craniotomy was performed under isoflurane anaesthesia (1–1.5%), and then a previously implanted head-plate was used to fix the mouse on a circular treadmill and the anaesthetic was removed. *In vivo* extracellular recordings were made from V1 and dLGN using multichannel silicon probes. Visual stimuli were displayed on an LCD screen. Microbial opsins were photoactivated using a blue (470-nm) or amber (590-nm) LED placed above the thinned skull. *In vitro* whole-cell recordings were performed as previously described³².

Full Methods and any associated references are available in the online version of the paper at www.nature.com/nature.

Received 29 August 2011; accepted 4 January 2012.

Published online 22 February 2012.

- Lorente de No, R. in *Physiology of the Nervous System* (ed. Fulton, J.F.) 274–301 (Oxford Univ. Press, 1943).
- Douglas, R. J. & Martin, K. A. Neuronal circuits of the neocortex. *Annu. Rev. Neurosci.* **27**, 419–451 (2004).
- Lefort, S., Tomm, C., Floyd Sarria, J. C. & Petersen, C. C. The excitatory neuronal network of the C2 barrel column in mouse primary somatosensory cortex. *Neuron* **61**, 301–316 (2009).
- Thomson, A. M. & Bannister, A. P. Interlaminar connections in the neocortex. *Cereb. Cortex* **13**, 5–14 (2003).
- Callaway, E. M. Local circuits in primary visual cortex of the macaque monkey. *Annu. Rev. Neurosci.* **21**, 47–74 (1998).
- Dantzker, J. L. & Callaway, E. M. Laminar sources of synaptic input to cortical inhibitory interneurons and pyramidal neurons. *Nature Neurosci.* **3**, 701–707 (2000).
- Thomson, A. M. Neocortical layer 6, a review. *Front. Neuroanat.* **4**, 13 (2010).
- Bourassa, J. & Deschenes, M. Corticothalamic projections from the primary visual cortex in rats: a single fiber study using biocytin as an anterograde tracer. *Neuroscience* **66**, 253–263 (1995).
- Binzegger, T., Douglas, R. J. & Martin, K. A. Stereotypical bouton clustering of individual neurons in cat primary visual cortex. *J. Neurosci.* **27**, 12242–12254 (2007).
- Zhang, Z. W. & Deschenes, M. Intracortical axonal projections of lamina VI cells of the primary somatosensory cortex in the rat: a single-cell labeling study. *J. Neurosci.* **17**, 6365–6379 (1997).
- Jones, E. G. *The Thalamus* (Cambridge Univ. Press, 2007).
- Guillery, R. W. & Sherman, S. M. Thalamic relay functions and their role in corticocortical communication: generalizations from the visual system. *Neuron* **33**, 163–175 (2002).
- Sillito, A. M. & Jones, H. E. Corticothalamic interactions in the transfer of visual information. *Phil. Trans. R. Soc. Lond. B* **357**, 1739–1752 (2002).
- Briggs, F. & Usrey, W. M. Emerging views of corticothalamic function. *Curr. Opin. Neurobiol.* **18**, 403–407 (2008).
- Cudeiro, J. & Sillito, A. M. Looking back: corticothalamic feedback and early visual processing. *Trends Neurosci.* **29**, 298–306 (2006).
- Sillito, A. M., Cudeiro, J. & Jones, H. E. Always returning: feedback and sensory processing in visual cortex and thalamus. *Trends Neurosci.* **29**, 307–316 (2006).
- Bolz, J. & Gilbert, C. D. Generation of end-inhibition in the visual cortex via interlaminar connections. *Nature* **320**, 362–365 (1986).
- Grieve, K. L. & Sillito, A. M. A re-appraisal of the role of layer VI of the visual cortex in the generation of cortical end inhibition. *Exp. Brain Res.* **87**, 521–529 (1991).
- Gong, S. *et al.* Targeting Cre recombinase to specific neuron populations with bacterial artificial chromosome constructs. *J. Neurosci.* **27**, 9817–9823 (2007).
- Nagel, G. *et al.* Channelrhodopsin-2, a directly light-gated cation-selective membrane channel. *Proc. Natl Acad. Sci. USA* **100**, 13940–13945 (2003).
- Boyden, E. S., Zhang, F., Bamberg, E., Nagel, G. & Deisseroth, K. Millisecond-timescale, genetically targeted optical control of neural activity. *Nature Neurosci.* **8**, 1263–1268 (2005).
- Niell, C. M. & Stryker, M. P. Highly selective receptive fields in mouse visual cortex. *J. Neurosci.* **28**, 7520–7536 (2008).
- Hubel, D. H. & Wiesel, T. N. Receptive fields, binocular interaction and functional architecture in the cat's visual cortex. *J. Physiol.* **160**, 106–154 (1962).
- Chow, B. Y. *et al.* High-performance genetically targetable optical neural silencing by light-driven proton pumps. *Nature* **463**, 98–102 (2010).
- Gradinaru, V. *et al.* Molecular and cellular approaches for diversifying and extending optogenetics. *Cell* **141**, 154–165 (2010).
- Rafols, J. A. & Valverde, F. The structure of the dorsal lateral geniculate nucleus in the mouse. A Golgi and electron microscopic study. *J. Comp. Neurol.* **150**, 303–331 (1973).
- Salinas, E. & Thier, P. Gain modulation: a major computational principle of the central nervous system. *Neuron* **27**, 15–21 (2000).
- Brotchie, P. R., Andersen, R. A., Snyder, L. H. & Goodman, S. J. Head position signals used by parietal neurons to encode locations of visual stimuli. *Nature* **375**, 232–235 (1995).
- Treue, S. & Martinez Trujillo, J. C. Feature-based attention influences motion processing gain in macaque visual cortex. *Nature* **399**, 575–579 (1999).
- McAdams, C. J. & Maunsell, J. H. Effects of attention on orientation-tuning functions of single neurons in macaque cortical area V4. *J. Neurosci.* **19**, 431–441 (1999).
- Silver, R. A., Lubke, J., Sakmann, B. & Feldmeyer, D. High-probability unquantal transmission at excitatory synapses in barrel cortex. *Science* **302**, 1981–1984 (2003).
- Adesnik, H. & Scanziani, M. Lateral competition for cortical space by layer-specific horizontal circuits. *Nature* **464**, 1155–1160 (2010).
- Markram, H. *et al.* Interneurons of the neocortical inhibitory system. *Nature Rev. Neurosci.* **5**, 793–807 (2004).
- Ascoli, G. A. *et al.* Petilla terminology: nomenclature of features of GABAergic interneurons of the cerebral cortex. *Nature Rev. Neurosci.* **9**, 557–568 (2008).
- Chance, F. S., Abbott, L. F. & Reyes, A. D. Gain modulation from background synaptic input. *Neuron* **35**, 773–782 (2002).
- Shadlen, M. N. & Newsome, W. T. The variable discharge of cortical neurons: implications for connectivity, computation, and information coding. *J. Neurosci.* **18**, 3870–3896 (1998).
- Murphy, B. K. & Miller, K. D. Multiplicative gain changes are induced by excitation or inhibition alone. *J. Neurosci.* **23**, 10040–10051 (2003).
- Andolina, I. M., Jones, H. E., Wang, W. & Sillito, A. M. Corticothalamic feedback enhances stimulus response precision in the visual system. *Proc. Natl Acad. Sci. USA* **104**, 1685–1690 (2007).
- Wang, W., Jones, H. E., Andolina, I. M., Salt, T. E. & Sillito, A. M. Functional alignment of feedback effects from visual cortex to thalamus. *Nature Neurosci.* **9**, 1330–1336 (2006).
- Wörgötter, F., Nelle, E., Li, B. & Funke, K. The influence of corticofugal feedback on the temporal structure of visual responses of cat thalamic relay cells. *J. Physiol.* **509**, 797–815 (1998).
- McClurkin, J. W. & Marrocco, R. T. Visual cortical input alters spatial tuning in monkey lateral geniculate nucleus cells. *J. Physiol.* **348**, 135–152 (1984).
- Murphy, P. C., Duckett, S. G. & Sillito, A. M. Feedback connections to the lateral geniculate nucleus and cortical response properties. *Science* **286**, 1552–1554 (1999).
- Casagrande, V. A. & Kaas, J. H. *The Afferent, Intrinsic and Efferent Connections of Primary Visual Cortex in Primates* (eds Peters, A. & Rockland, P.) (Plenum, 1994).

Supplementary Information is linked to the online version of the paper at www.nature.com/nature.

Acknowledgements We are grateful to M. Carandini, J. Isaacson and the members of the Scanziani and Isaacson laboratories for helpful discussions of this project, to J. Isaacson, R. Malinow and T. Korniyama for providing feedback on the manuscript, to P. Abelkop for histological help and neonatal viral injections, to J. Evora for mouse colony support and genotyping, to B. Atallah for sharing the technique for silencing the cortex by photostimulation of parvalbumin neurons and for help with the *in vivo* recording setup and to W. Bruns for help coding analysis software. We thank the UCSD Neuroscience Microscopy Facility (P30 NS047101) for the use of their imaging equipment. S.R.O. and H.A. were supported by postdoctoral fellowships from the Helen Hay Whitney Foundation. D.S.B. was supported by a UCSD Neurobiology Training Grant (NINDS: 5T32NS007220-28). M.S. is an investigator of the Howard Hughes Medical Institute. This work was also supported National Institutes of Health grant R01 NS069010 and by the Gatsby Charitable Foundation.

Author Contributions H.A. performed the initial physiological characterization of the NTSR1-Cre expression system with optogenetic tools. H.A. also developed the *in vivo* awake recording preparation on the treadmill. S.R.O. performed all *in vivo* recordings. D.S.B. performed all *in vitro* recordings and anatomical reconstructions. S.R.O. and M.S. designed the study. M.S. wrote the paper.

Author Information Reprints and permissions information is available at www.nature.com/reprints. The authors declare no competing financial interests. Readers are welcome to comment on the online version of this article at www.nature.com/nature. Correspondence and requests for materials should be addressed to M.S. (massimo@biomail.ucsd.edu) or S.R.O. (srolsen@ucsd.edu).

METHODS

All procedures were conducted in accordance with the National Institutes of Health guidelines and with the approval of the Committee on Animal Care at the University of California, San Diego.

Animals. We used the following mouse lines: NTSR1-Cre (strain B6.FVB(Cg)-Tg(Ntsr1-cre)GN220Gsat/Mmcd, stock number 030648-UCD), which was generated by the GENSAT project¹⁹ and acquired from the Mutant Mouse Regional Resource Centers; tdTomato reporter (Jax number 007908); GAD67-GFP (Aneo); and PV-Cre (Silvia Arber).

Viral injections. Adeno-associated viruses (AAVs) for ChR2 and archaerhodopsin were acquired from the University of Pennsylvania Viral Vector Core: AAV2/1.CAGGS.flex.ChR2.tdTomato.SV40 (Addgene 18917) and AAV2/9.flex.CBA.Archaerhodopsin-GFP.W.SV40 (Addgene 22222). An AAV virus (AAV2/9) for NpHR3.0 was produced at the Salk Viral Vector Core. The NpHR3.0 plasmid (pAAV-Efla-DIO-eNpHR 3.0-EYFP) was provided by K. Diesseroth.

Viruses were loaded in a bevelled sharp micropipette mounted on a Nanoject II (Drumond) or a micropump injector (UMP-3 WPI) attached to a micromanipulator. ChR2 virus was injected into newborn pups (between postnatal days 0 and 2) that were anaesthetized on ice and secured into a moulded platform. Three 20-nl boli of virus was injected at each of three medial-lateral locations in V1 and two depths (500 μm and 650 μm) within V1.

Archaerhodopsin was injected in combination with NpHR3.0 in juvenile (1–2-month-old) mice anaesthetized with 2.5% isoflurane and placed into a stereotaxic frame (Knopf). The exposed skull overlying V1 was thinned in three locations with a dental drill (Foredom) with a 300- μm bur (Gesswein), and a hole was made with a (25-gauge) needle at each location to permit insertion of the injection pipette. A volume of 150 nl of virus was injected at a rate of 20 nl min⁻¹ at each of the three locations and at two depths (900 μm and 700 μm). The scalp was then sutured and the mouse injected subcutaneously with 0.1 mg kg⁻¹ buprenorphine. *In vivo* recordings were made 1–2 months after viral injection.

Slice preparation. Mice were anaesthetized with ketamine and xylazine (100 mg kg⁻¹ and 10 mg kg⁻¹, respectively), perfused transcardially with cold sucrose solution (in mM: NaCl, 83; KCl, 2.5; MgSO₄, 3.3; NaH₂PO₄, 1; NaHCO₃, 26.2; D-glucose, 22; sucrose, 72; and CaCl₂, 0.5, bubbled with 95% O₂ and 5% CO₂) and decapitated, and the visual cortex was cut into 300–400- μm coronal sections in cold sucrose solution. Thalamic slices were cut 45° off the coronal plane to maintain connections between NRT and dLGN. Slices were incubated in sucrose solution in a submerged chamber at 34 °C for 30 min and then at room temperature (21 °C) until used for recordings.

***In vitro* recordings.** Whole-cell recordings were done at 32 °C in artificial cerebrospinal fluid (in mM: NaCl, 119; KCl, 2.5; NaH₂PO₄, 1.3; NaHCO₃, 26; D-glucose, 20; MgCl₂, 1.3; CaCl₂, 2.5; and mOsm, 305, bubbled with 95% O₂ and 5% CO₂). Excitatory and inhibitory synaptic currents were recorded using a caesium-based internal solution (in mM: CsMeSO₄, 115; NaCl, 4; HEPES, 10; Na₃GTP, 0.3; MgATP, 4; EGTA, 0.3; QX-314-Cl, 2.5; BAPTA(5Cs), 10; adjusted to pH 7.4 with CsOH; mOsm 295; 3–5 MOhm pipette resistance). Voltage-clamp recordings were not considered if the series resistance exceeded 20 MOhm or varied by more than 10%. Typically, 2–4 neurons were recorded from simultaneously. Cell-attached recordings and biocytin fills were carried out with a potassium-based internal solution (in mM: K-gluconate, 150; MgCl₂, 1.5; HEPES, 5; EGTA, 1.1; phosphocreatine, 10; adjusted to pH 7.4 with KOH; mOsm 295). Perforated-patch recordings were carried out using potassium-based internal and 10 $\mu\text{g ml}^{-1}$ Gramicidin D (Sigma G5002). Tight seals were held until sufficient access allowed injection of current and resolution of action potentials (typically 10–20 min). Ruptures of the perforated patch were apparent by a rapid drop in series resistance at which point the recordings were discontinued. Photostimulation of L6 *in vitro* consisted of either single 2-ms pulses or a 40-Hz train of 2-ms pulses, or of 1-s ramps of light of increasing intensity as previously described³². Data were recorded with Multiclamp 700B amplifiers (Axon instruments) filtered at 2 kHz and digitized with a Digidata1440A (Axon instruments) at 10 kHz. Recordings were analysed using custom-made routines in Igor Pro (Wavemetrics). Charges represent the time integral of the synaptic current recorded during the first second of photostimulation. The stage was moved using a custom made plugin for ImageJ(NIH) to interface with ESP300 (Newport) via SerialPort (SerialIO). Drugs used were NBQX (Tocris 1044) and CPP (Ascent Asc-159).

***In vivo* recordings in anaesthetized mice.** Recordings were performed similarly to those previously described²². Animals were anaesthetized with 5 mg kg⁻¹ of chlorporthixene (intraperitoneal) and then (5–10 min later) with 1.2 g kg⁻¹ urethane (intraperitoneal). During surgery, animals were given 0.5–1.0% isoflurane. Animals were placed onto a custom platform and their temperature was maintained at 37 °C using a feedback-controlled heating pad (FHC). Whiskers and eyelashes that were contralateral to the recording side were trimmed and eyes covered with a

thin, uniform layer of silicone oil to prevent drying. Protein expression was verified by transcranial epifluorescence of the exposed and PBS-moistened skull using a Leica MZ10F microscope. Only animals showing expression over the entire extent of V1 were used for subsequent experiments. The entire dried skull was covered with black dental cement (Ortho-Jet powder (Lang Dental) mixed with black iron oxide) but for the previously outlined boundaries of V1 (~1.5–3.5 mm lateral to midline and -0.5 to 2.5 mm anterior to lambda suture). A head-plate with a hole of ~2 mm in diameter was mounted over V1 and a small region of skull (~300 × 750 μm) was thinned using a dental drill. Next, we used sharpened fine forceps (Dumont number 55) to make a craniotomy just sufficiently large for inserting the probe. A drop of PBS placed in the well at the centre of the head-plate kept the exposed skull and craniotomy moist. A multichannel silicon probe mounted on a micromanipulator (Luigs-Neumann) was slowly advanced into the brain to a depth of 800–1000 μm for linear probes and 200–700 μm for tetrode probes (see later), and recordings were started 20 min or more after inserting the probe.

For dLGN recordings we made a circular craniotomy (~1.5 mm in diameter) 2.6 mm posterior and 2 mm lateral to the bregma suture. Robust visual responses and bursting activity that was characteristic of dLGN relay neurons were encountered at a depth between 2,400 and 3,100 μm^4 (Supplementary Fig. 7). For dual recording experiments (Fig. 3g, h and Fig. 5), we used a larger head-plate so that a craniotomy could be made both over the dLGN and V1.

Recordings were made with NeuroNexus 16-channel linear (a1x16-3mm-50-177) or tetrode (a2x2-tet-3mm-150-121) silicon probes. For recordings across cortical depth and in dLGN we used the linear configuration. The tetrode configuration was used to isolate a subset of cells in Fig. 2. Signals were amplified ×1000, band-pass filtered between 0.3 Hz and 5 kHz using an AM Systems 3500 amplifier and acquired at 32 kHz using a NIDAQ board (PCIe-6239) controlled with custom-written software in Matlab (Mathworks). For dual recording experiments we used two separate data-acquisition setups (amplifier, NIDAQ board and computer). Raw data were stored on a computer hard drive for offline analysis.

At the end of the recording session, animals were killed by administering 4% isoflurane and the brain was quickly removed and fixed in 4% paraformaldehyde for histological analysis.

***In vivo* awake recordings.** 1–2 weeks before recording, mice were implanted with a head-plate for head fixation. Mice were anaesthetized with 2.5% isoflurane, the scalp was removed and a head-plate was fixed over V1 with black dental cement. The skull directly overlying V1 was covered with Kwik-Cast (WPI). Animals were injected subcutaneously with 0.1 mg kg⁻¹ buprenorphine and allowed to recover in their home cage for at least 1 week before recording.

Several days before recording, mice were familiarized to head fixation within the recording setup. They were briefly anaesthetized with isoflurane and the head-plate was clamped to a metal post, but otherwise the mice were unrestrained and allowed to run in this position on a plastic circular treadmill or track (Fast-Trac from Bio-Serv; see Supplementary Fig. 6). The same circular track was present in the cages of the mice, where they were familiarized with its use. Mice grew accustomed to head fixation over the course of 1–3 15-min sessions and ran naturally on the track, occasionally stopping to rest or groom.

On the day of recording, mice were anaesthetized with 1.5–2% isoflurane, a small craniotomy was made over V1, a drop of PBS was placed in the well of a head-plate that was clamped to a metal post, and the multichannel probe inserted into the craniotomy. After removal of isoflurane the mice regained consciousness and typically began running. Recordings did not start before 30 min after the end of anaesthesia. Awake recording sessions lasted between 1 and 2 h. Mice typically spent ~60–80% of their time running, and the rest of the time was spent resting or grooming. Data were not separated according to behaviour. Every 30–60 min mice were given a few drops of a 5% glucose solution through a disposable pipette. For two mice we performed 2–3 recording sessions, which were made at least a day apart. Between sessions the craniotomy was covered with Kwik-Cast. A new craniotomy was made for each session.

Visual stimulation. Visual stimuli were generated in Matlab using the Psychophysics Toolbox⁴⁵ and were displayed on a gamma-corrected LCD monitor (Dell 52 × 32.5 cm, 60-Hz refresh rate, mean luminance 50 cd m⁻²) positioned 25 cm from the contralateral eye. The monitor was positioned for each experiment so that the multi-unit receptive field was located approximately in the centre of the screen (the multi-unit receptive field was determined by moving a localized drifting grating patch (~10°) around the screen). During the recording session full-field sinusoidal drifting gratings were used. All stimuli had a temporal frequency of 2 Hz and a spatial frequency of 0.04 cycles per degree. Gratings were randomly presented at 8–12 equally spaced directions, except for the experiments in Fig. 5 in which we used only two orthogonal grating directions (0° and 90°). The contrast of the stimulus was 100%, except for Fig. 5 in which we used six contrast levels (2, 4.4,

9.6, 21, 46 and 100%). A grey screen trial was interleaved with the drifting gratings. The duration of the visual stimulus was 1.5 s and the inter-trial interval was 3–6 s. **In vivo photostimulation.** To photo-stimulate Chr2 we used a blue (470-nm) fibre-coupled LED (1 mm diameter, Doric Lenses) placed ~5–10 mm away from the skull. Light from the LED spanned the entire area of V1. An opaque shield of black aluminium foil (Thor Labs) prevented LED light from reaching the contralateral eye. The LED was driven by the analogue output from the NIDAQ board. The blue LED was presented at five intensities (approximately 3, 5, 7, 10.5 and 20 mW measured at the tip of the fibre), but for a minority of experiments we presented only the highest LED intensity. Trials were alternated between visual stimulus only and visual stimulus plus LED. The strongest LED intensity also generated oscillations at gamma frequency, consistent with previous observations³² (Supplementary Fig. 2). The preferred-orientation of photostimulated L6 cells remained unchanged but their tuning curves became broader (Supplementary Fig. 2).

To photostimulate archaerhodopsin and NpHR3.0 we used an amber (590-nm) fibre-coupled LED (1 mm in diameter, Doric Lenses) placed ~0.5 mm from the skull. Because photosuppression of L6 produced a transient decrease in spontaneous multi-unit activity in L2–5 at the onset of LED illumination (see Supplementary Fig. 6) we turned on the amber LED 1.4 s before the visual stimulus began. Experiments were performed at the highest LED intensity (~20 mW measured at the tip of the fibre). As long as the suppression was not complete, the preferred orientation of photosuppressed L6 cells remained unchanged (Supplementary Fig. 6). **In vivo data analysis.** All *in vivo* data analysis was performed with custom software written in Matlab.

Multi-unit spiking activity was defined as all events (spikes) exceeding a threshold of 4 s.d. above the noise of the high-pass filtered (500-Hz) signal. Spikes were assigned a depth corresponding to the depth of the channel they were recorded from. Spikes that were recorded simultaneously on multiple channels were considered as a single event and attributed to the channel in which they showed the largest amplitude. We determined the depth of each channel by considering the depth and the angle of the probe relative to the vertical axis of cortex. We assigned spikes to different layers according to the following depths (in μm): L2/3, 100–350; L4, 350–450; L5, 450–650; L6, >650. PSTHs were composed of 50-ms bins. PSTHs of individual experiments were normalized to the first 500 ms of the visual stimulus (for Chr2 experiments) or to the entire visual stimulus (for archaerhodopsin and NpHR3.0 experiments) to generate average PSTHs. PSTHs for kinetic analysis (Fig. 3h) were composed of 3-ms bins and report the normalized difference in firing rates between control (average firing over a 50-ms window prior to LED onset) and during LED illumination (average firing rate over a 100-ms window, 50 ms after LED onset). For each experiment the onset of suppression was determined as the time point at which the normalized response fell below 2 s.d. of the baseline.

The contrast response functions in dLGN and V1 report the normalized, baseline-subtracted firing rates and were fitted with a hyperbolic ratio function:

$$r = r_{\max} \frac{c^n}{c^n + c_{50}^n}$$

where r is the response, c is the contrast of the visual stimulus, r_{\max} is a fitted constant representing the response saturation level, n is fitting exponent that affects the shape of the curve and c_{50} is the semi-saturation constant. The transfer function between the dLGN and V1 was fitted with a hyperbolic ratio function:

$$r_{V1} = r_{V1, \max} \frac{r_{\text{dLGN}}^n}{r_{\text{dLGN}}^n + r_{\text{dLGN}, 50}^n}$$

where r_{V1} is the V1 response, $r_{V1, \max}$ is a constant representing the V1 saturation level, r_{dLGN} is the dLGN response, n is a fitting exponent and $r_{\text{dLGN}, 50}$ is the semi-saturation constant. The ‘corticothalamic component’ (CT) was defined as the fraction of the total V1 suppression accounted for by this predicted response. The ‘intracortical component’ was then defined as 1–CT component. We performed this analysis for five LED levels and averaged across experiments to produce the plot in Fig. 5f.

We isolated single units using spike-sorting software provided by D. N. Hill, S. B. Mehta, and D. Kleinfeld⁴⁶. For both the linear and tetrode probes we analysed waveforms extracted from groups of four adjacent electrode sites. We high-pass filtered the raw signal at 500 Hz and then detected spiking events exceeding 4–5 s.d. of the noise. Spike waveforms were clustered using a k -means algorithm. After initial automated clustering, we used a graphical user interface to manually merge

and split clusters. Unit isolation quality was assessed by considering refractory period violations and Fisher linear discriminant analysis. In agreement with previous studies we could classify waveforms as regular-spiking or fast-spiking putative inhibitory neurons. In our data set there was a clear bimodal distribution of trough-to-peak times (a threshold of 0.4 ms was used to divide fast-spiking from regular-spiking units). All units were assigned a depth according to the channel that they were detected on, and units were assigned to layers based on the depth divisions given above for the multi-unit activity.

For each unit we computed the visual response as the mean spike-rate occurring over the time window in which both the LED and visual stimulus were present. Thus, for the L6 photostimulation experiments this typically corresponded to a 500-ms window placed in the centre of the visual response, and for the L6 photosuppression experiments this window encompassed the entire 1.5-s visual stimulus. For all analysis except the orientation tuning analysis in Fig. 2, we averaged responses over all stimulus conditions. Following recent studies^{47,48} of orientation tuning we computed an OSI as:

$$\text{OSI} = \frac{\sqrt{(\sum r_k \sin(2\theta_k))^2 + (\sum r_k \cos(2\theta_k))^2}}{\sum r_k}$$

where r_k is the response to the k th direction given by θ_k . We determined an OSI for each unit with and without photostimulation or suppression of L6. We established the preferred orientation and tuning width by first fitting the average responses of each unit with a sum of two Gaussians:

$$r = r_0 + r_p e^{-(\theta - \theta_p)^2 / (2\sigma^2)} + r_{p+180} e^{-(\theta - \theta_p - 180)^2 / (2\sigma^2)}$$

where r_0 is a constant offset, r_p is the response at the preferred orientation, r_{p+180} is a response 180° away from the preferred direction, θ is the stimulus direction, θ_p is the preferred orientation and σ is the tuning width. The two Gaussians were forced to peak 180° apart and to have the same width but could have different amplitudes. Control and photostimulation or photosuppression conditions were fit separately. To generate the average population tuning curve we first circularly shifted the stimulus direction of each unit so that the maximal response occurred at 0°. We then normalized the responses to this peak response and averaged all normalized tuning curves together. We fit the control population average tuning curve with a sum of two Gaussians. The curve for the photostimulation or photosuppression population average was produced by scaling the control curve by the slope (gain factor) of the linear fit shown in Fig. 2e, j.

All error bars are presented as mean \pm s.e.m. unless otherwise noted. We used paired t -tests to assess statistical significance unless otherwise noted.

Histology. Triple transgenic mice (Ntsr1-Cre, floxed-tdTomato and Gad67-GFP) were anaesthetized with ketamine and xylazine (100 mg kg⁻¹ and 10 mg kg⁻¹, respectively) and perfused with cold sucrose (see above) and then perfluoroalkoxy (4% in PBS). After 24 h incubation in perfluoroalkoxy, slices were cut into 50- μm sections and immunostained as described previously⁴⁹. Antibodies that were used were mouse anti-NeuN (1:400; Millipore MAB377), chicken anti-GFP (1:1000; Aves Labs GFP-1020), goat anti-chicken AF488 (1:1,000; Invitrogen A11039) and goat anti-mouse AF633 (1:1,000; Invitrogen A21050). Slices were mounted in Vectashield with Dapi (Vector Labs, H1500). Images were single confocal sections taken on an Olympus FV1000. Layer borders were identified by changes in cell density. Cell counts were carried out using standard stereological techniques. Biocytin fills and neural reconstructions were done as previously described⁵⁰.

44. Grubb, M. S. & Thompson, I. D. Quantitative characterization of visual response properties in the mouse dorsal lateral geniculate nucleus. *J. Neurophysiol.* **90**, 3594–3607 (2003).
45. Brainard, D. H. The psychophysics toolbox. *Spat. Vis.* **10**, 433–436 (1997).
46. Fee, M. S., Mitra, P. P. & Kleinfeld, D. Automatic sorting of multiple unit neuronal signals in the presence of anisotropic and non-Gaussian variability. *J. Neurosci. Methods* **69**, 175–188 (1996).
47. Kerlin, A. M., Andermann, M. L., Berezovskii, V. K. & Reid, R. C. Broadly tuned response properties of diverse inhibitory neuron subtypes in mouse visual cortex. *Neuron* **67**, 858–871 (2010).
48. Ringach, D. L., Shapley, R. M. & Hawken, M. J. Orientation selectivity in macaque V1: diversity and laminar dependence. *J. Neurosci.* **22**, 5639–5651 (2002).
49. Bortone, D. & Polleux, F. KCC2 expression promotes the termination of cortical interneuron migration in a voltage-sensitive calcium-dependent manner. *Neuron* **62**, 53–71 (2009).
50. Bagnall, M. W., Hull, C., Bushong, E. A., Ellisman, M. H. & Scanziani, M. Multiple clusters of release sites formed by individual thalamic afferents onto cortical interneurons ensure reliable transmission. *Neuron* **71**, 180–194 (2011).